

cently though, [Schultheis et al. \(2015\)](#) find the presence of a metal-poor population beyond 70 pc from the nuclear cluster, which has a radius of approximately 7 pc ([Fritz et al. 2016](#)). [Do et al. \(2015\)](#) also report a significant population of metal-poor stars in the nuclear cluster.

Here we report on the first high-resolution spectroscopy of a red giant with $[\text{Fe}/\text{H}] \sim -1$ to be found in the vicinity of the nuclear cluster, at a projected distance of 1.5 pc from the Galactic Center. We have performed a detailed abundance analysis based on high-resolution, K-band spectra. Observing at K band make such investigations possible due to the much lower extinction at higher wavelengths ([Cardelli et al. 1989](#)). The K band extinction toward the central parsec is only $A_{K_S} = 2.74$ with a variation of ± 0.30 due to spatial variations ([Schödel et al. 2010](#)).

2. TARGET SELECTION

We selected a list of Galactic Center giants from spectra observed with the integral field spectrometer SINFONI ([Eisenhauer et al. 2003](#); [Bonnet et al. 2003](#)) on the VLT, providing a K-band resolution of $R = 4000$ or $R = 1500$. The selection for the target group, to which the observed star belongs, was done according to following criteria: a K_S magnitude range of $10 < K_S < 11$, an angular distance from the Galactic Center of $R_c(\text{SgrA}^*) > 25''$, and excluding stars with neighbors too close for seeing-limited high resolution spectroscopy. Initially, SINFONI spectra were only used to ensure qualitatively that the objects are cool in the sense that the CO band-heads exist, but we have not imposed any initial cuts based on the CO band strength or derived effective temperature. We also used the catalogs of [Blum et al. \(2003\)](#); [Matsunaga et al. \(2009\)](#) to exclude some known AGB/LPV stars like Miras, and known red supergiants. The aim of this sample is to develop a relatively unbiased, large sample of old Galactic Center stars that we will use in our study of the metallicity distribution. A more detailed discussion of our full sample is in preparation.

In [Figure 1](#) we present a finding chart ([Lawrence et al. 2013](#)) with our observed target, the giant GC10812, indicated (see also [Table 1](#)). The star lies at an angular distance of $38.4''$ from the Galactic Center. This corresponds to a projected galactocentric distance of $R_c = 1.5$ pc, adopting the distance to the Galactic Center of 8.3 kpc ([Chatzopoulos et al. 2015a](#); [Bland-Hawthorn & Gerhard 2016](#)).

The K_S magnitude of GC10812 is 10.25 ± 0.05 from [Nishiyama et al. \(2009\)](#) and its color is $H - K_S = 1.63 \pm 0.07$. Using the extinction law of [Fritz et al. \(2011\)](#) this leads to an extinction of $A_{K_S} = 1.94 \pm 0.10$. The absolute magnitude of GC10812 is $M_{K_S} = -6.48 \pm 0.12$.

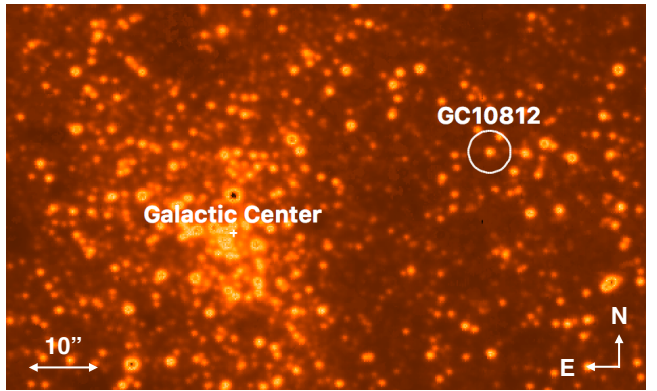


Figure 1. UKIDSS finding chart of the Galactic center ([Lawrence et al. 2013](#)). GC10812 is marked with a circle.

This is close to the approximate tip of the RGB with $M_{bol} = -3.5$ (see also [Tiede et al. \(1995\)](#), [Omont et al. \(1999\)](#)). Compared to all stars brighter than $M_{K_S} = -5.5$ from [Nishiyama et al. \(2009\)](#) within $100''$ of Sgr A* the star is clearly bluer, -0.84 bluer than the median color. That means that only 21 of 1067 stars are bluer than GC10812. There are also extinction variations over the Galactic Center ([Schödel et al. 2010](#)). To account for them we measure relative color locally using Gemini AO data¹. We use stars with $K_S < 16$ and account for intrinsic color differences. Dependent on the comparison scale (3 or $6''$) and including other error sources like scatter and photometry uncertainty for the target we obtain that GC10812 is 0.75 ± 0.10 bluer than the local median. Over the full Galactic Center $3.6^{+2.7}_{-1.9}\%$ of all stars are that blue or bluer. The $H - K_S$ color excess corresponds to an extinction difference of $A_{K_S} = 1.01 \pm 0.14$ between the $A_{K_S} = 1.94$ measured for this star and $A_{K_S} = 2.95$ measured as the average for all stars in this region. That is more dust than the $A_{K_S} \approx 0.4$ which [Chatzopoulos et al. \(2015b\)](#) find within $r = 100''$ of Sgr A*. However, there is also extinction variation in the plane of sky ([Schödel et al. 2010](#)), at some places up to $A_{K_S} \approx 0.8$ were found. Further, the model of [Chatzopoulos et al. \(2015b\)](#) is very insensitive to dust at greater distances.

To constrain the line of sight position, we use the Galactic Center model of [Chatzopoulos et al. \(2015a\)](#) and derive how much a star needs to be placed in front of Sgr A* in order for it to be bluer than $3.6^{+2.7}_{-1.9}\%$ of its stars. We obtain a distance of $D_c = 26^{+54}_{-16}$ parsec. That is in principle a slight underestimate of the distance because the model includes no bar-bulge nor Galactic disc. This contribution is, however, probably

¹ We use H-continuum and K (long) continuum images from program Gs-2013A-Q-15 avoiding data in which the target is saturated.

small; Launhardt et al. (2002) show that in this part of the nuclear disk the space density due to the bar/bulge is more than 40 times smaller than the contribution due to the nuclear disk. Its absolute extinction also argues for a location within the nuclear disk; an extinction of $A_{K_s} \approx 2$ is unusual for old stars outside the nuclear disk (Schultheis et al. 2014). Whether it is possible that the star still is around the outer rim of the nuclear cluster or not, depends on the precise distance and nuclear cluster definition (Schödel et al. 2014; Chatzopoulos et al. 2015a; Fritz et al. 2016). It is however clear that the star is currently within a nuclear component, because the nuclear disk extends to an outer radius of 230 pc (Launhardt et al. 2002).

The dynamics measured in Fritz et al. (2016) are $\mu_l = 2.31 \pm 0.27 \text{ mas yr}^{-1}$, $\mu_b = -3.12 \pm 0.27 \text{ mas yr}^{-1}$, and $v_{rad} = -51 \pm 5 \text{ km s}^{-1}$ (which we confirm in our measurement of the star’s heliocentric velocity from the NIRSPEC high-resolution spectra of $-56.4 \pm 1.0 \text{ km s}^{-1}$, see Table 1). These velocities are rather typical for a Galactic Centre star, see Figure 2. The positive velocity in l and the lower extinction fits as the extinction to a star in front of the Galactic Center (Chatzopoulos et al. 2015b).

We calculate the orbit for the stars using the potential of Chatzopoulos et al. (2015a). This potential includes the supermassive black hole, nuclear cluster, and cluster disk. Three orbits are shown in Figure 3. For small current distances (black and red orbits in the Figure) the average distance of GC10812 from the Galactic Center is somewhat larger than the current distance from the Galactic Center. That makes membership in the nuclear cluster unlikely, and excludes it nearly certainly if the cluster is assumed to have a Sersic like cutoff, which results in a half light radius of about 5 pc (Fritz et al. 2016; Schödel et al. 2014). If it is instead assumed that the outer slope follows a power law (Chatzopoulos et al. 2015a), a membership in the nuclear cluster is still possible. When the star is currently at large distance (blue orbit in Figure 3), the star does not move much further away on its orbit. We conclude that the star most likely resides within the the nuclear disk and is unlikely to experience any excursions into the bulge or halo. We conclude based on the distance and kinematics that GC10812 is probably a nuclear disk star.

3. OBSERVATIONS

We observed the giant GC10812 on April, 27 2015 with the NIRSPEC spectrometer McLean (2005) mounted on Keck II, at a resolution of $R \sim 24,000$ in the K band, using the $0.432'' \times 12''$ slit and the NIRSPEC-7 filter. The retrieved spectra range from 21,100 to 23,300 Å, using 5 orders and therefore obtaining about 50% spectral coverage. We observed in an ABBA scheme with a

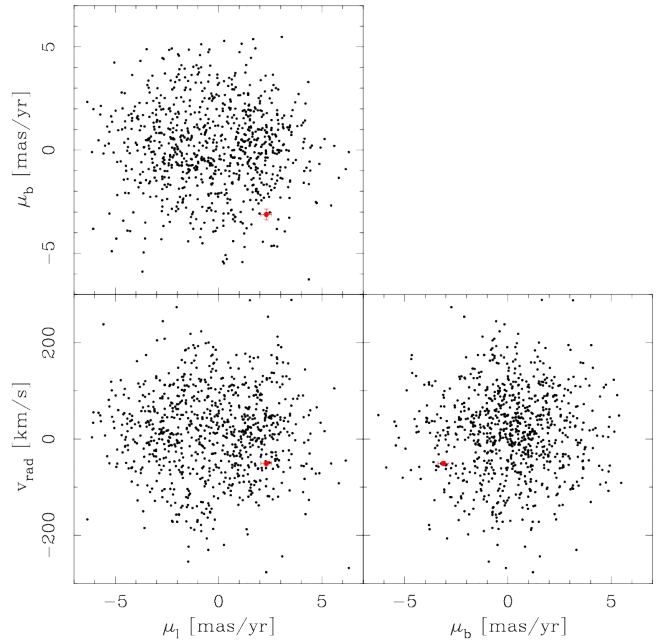


Figure 2. Velocity of GC10812 (red) in comparison with other Galactic Center stars. The other stars are in 0.8 to 3.6 pc projected distance from Sgr A*

nodding throw of $6''$ on the slit, to achieve proper background and dark subtraction. A total exposure time on target was 960 s. The data were reduced with the NIRSPEC software redspec (Kim et al. 2015) providing final 1-D wavelength-calibrated spectra. IRAF (Tody 1993) was subsequently used to normalize the continuum, eliminate obvious cosmic ray hits, and correct for telluric lines (with telluric standard stars). We estimate $S/N=90$ per pixel in our reduced spectra. A portion of the observed spectrum is shown in Figure 4.

4. ANALYSIS

We analyze our spectra, deriving detailed chemical abundances, by calculating synthetic spectra, given the star’s fundamental parameters, i.e. effective temperature (T_{eff}), surface gravity ($\log g$), metallicity ($[\text{Fe}/\text{H}]$), and microturbulence (ξ_{mic}) and a suitable line list in the K band (see Sect. 4.2)

4.1. The stellar parameters

The derived $T_{\text{eff}} = 3817 \pm 150 \text{ K}$, is determined from integrating the strength of the $2.3\mu\text{m}$ (2-0)CO band in the SINFONI spectra² and using the relation between the CO-band strength and the T_{eff} given in Schultheis et al. (2016). They have shown that this relation works very well in the temperature range between 3200 K and 4500 K and in the metallicity range between 0.5 dex and -1.2 dex with a typical dispersion of about 150 K.

² The SINFONI spectrum is from program 087.B-0117.

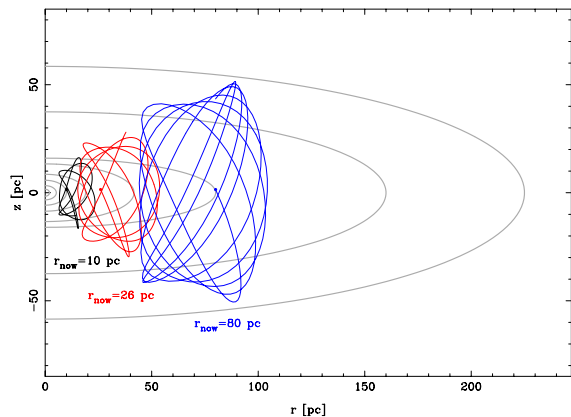


Figure 3. Orbit of GC10812. The red curve shows it for the most likely distance in front of the Galactic Center (26 pc), while the other two curves show the orbit when the star would be at the outer/inner edge of the one sigma interval. The gray curves show equal star surface density contours of the nuclear disk from [Fritz et al. \(2016\)](#); [Launhardt et al. \(2002\)](#). The outer most curve marks roughly the outer edge of the nuclear disk.

The surface gravity, $\log g$, is determined photometrically and assuming a mean distance of 8.3 kpc to the Galactic Center, in the same manner as in [Ryde & Schultheis \(2015\)](#). A stellar mass of an old star of typically $1 M_{\odot}$ is assumed, but the surface gravity is not very sensitive to the mass. A difference in mass of $0.2 M_{\odot}$ gives 0.1 dex $\log g$ difference. In the calculation of the surface gravity we used the extinction law from [Fritz et al. \(2011\)](#), and the bolometric corrections from [Houdashelt et al. \(2000\)](#). An extinction uncertainty of $A_{K_s} = 0.1$ gives 0.2 dex error in $\log g$ and a bolometric uncertainty of $M_{\text{bol}} = 0.12$ gives 0.15 dex uncertainty in $\log g$. The combined uncertainty is thus $\sqrt{0.1^2 + 0.2^2 + 0.15^2} = 0.27$ dex. Our derived surface gravity is thus $\log g = 0.5 \pm 0.3$ (dex).

[Ramírez et al. \(2000a\)](#) found that the combination of the CO first overtone band together with the Na I and the Ca I lines are sensitive to the surface gravity of the star. We have therefore also measured the Na I and the Ca I lines in the SINFONI spectra as in [Schultheis et al. \(2016\)](#). Our derived value for $\log [\text{EW}(\text{CO})/(\text{EW}(\text{Na}) + \text{EW}(\text{Ca}))] = 0.405$ for GC10812 locates our star on the RGB sequence of [Ramírez et al. \(1997\)](#).

We have chosen a typical value of $\chi_{\text{mic}} = 2.0 \pm 0.5$ km s^{-1} found in detailed investigations of red giant spectra in the near-IR by [Tsuji \(2008\)](#), see also the discussion in [Cunha et al. \(2007\)](#).

The location of GC10812 in the Hertzsprung-Russel diagram, using our derived effective temperature, surface gravity, and metallicity (see Table 2), is plotted

with a big star symbol in Figure 6. It fits nicely on the red-giant branch.

4.2. Line list

An atomic line list based on the VALD3 database ([Piskunov et al. 1995](#); [Kupka et al. 1999](#); [Ryabchikova et al. 1997](#); [Kupka et al. 2000](#); [Ryabchikova et al. 2015](#)) has been constructed ([Thorsbro et al. 2017, in prep.](#)). Wavelengths and line-strengths (astrophysical $\log gf$ -values) are updated for 575 lines in the K band using the solar center intensity atlas ([Livingston & Wallace 1991](#)). New laboratory measurements of wavelengths and oscillator strengths of Sc lines ([Pehlivan et al. 2015](#)) and newly calculated oscillator strengths of Mg lines ([Pehlivan et al. 2016, in prep](#)) are included. ABO³ line-broadening theory is included ([Anstee & O’Mara 1991](#); [Barklem & O’Mara 1998](#)) when available. In the abundance analysis, we also include molecular line-lists of CN ([Jørgensen & Larsson 1990](#)) and CO ([Goorvitch 1994](#)).

The line list is tested by determining abundances from high-quality spectra of α Boo ([Hinkle et al. 1995](#)) and 5 thick-disk stars. The thick-disk giants were observed with NIRSPEC in the same manner as for GC10812. The parameters and abundances of α Boo are from [Ramírez & Allende Prieto \(2011\)](#) and of the thick disk stars from the APOGEE pipeline ([Ahn et al. 2014](#)). The parameter range of these test stars are $4150 < T_{\text{eff}}/\text{K} < 4750$, $1.5 < \log g < 2.5$, and $-0.5 < [\text{Fe}/\text{H}] < -0.1$. We find an excellent agreement, to within 0.05 dex, between the abundances we determined from the K band and these reference values. The line list has not yet been tested against super-solar metallicity stars. Thus, the line list can with confidence be used for metal-poor to solar-metallicity cool stars.

4.3. Spectral synthesis

We derive our target star’s abundances by comparing the observed spectrum with synthesised spectra using the software *Spectroscopy Made Easy*, SME ([Valenti & Piskunov 1996, 2012](#); [Piskunov & Valenti 2016](#)). This program uses a grid of model atmospheres (MARCS spherical-symmetric, LTE model-atmospheres ([Gustafsson et al. 2008](#))) in which it interpolates for a given set of fundamental parameters of the analysed star. The spectral lines, which are used for the abundance analysis, are marked with masks in the pre-normalized observed spectra. SME then iteratively synthesizes spectra for the searched abundances, under a scheme to minimize the

³ ABO stands for Anstee, Barklem, and O’Mara, authors of the papers describing the theory in [Anstee & O’Mara \(1991\)](#); [Barklem & O’Mara \(1998\)](#)

χ^2 when comparing with the observed spectra. In order to match our synthetic spectra with the observed ones, we also convolve the synthetic spectra with a Gaussian

function of FWHM of $20 \pm 0.5 \text{ km s}^{-1}$. This broadening accounts for the instrumental spectral resolution and the macroturbulence of the stellar atmosphere.

Table 1. Stellar coordinates, position, and kinematics

Data	RA [h:m:s]	dec [d:m:s]	(l, b) [$^\circ, ^\circ$]	R_c [pc]	D_c [pc]	$v_{\text{rad}}^{\text{helio}}$ [km s^{-1}]	μ_l mas yr^{-1}	μ_b mas yr^{-1}
GC10812	17 : 45 : 37.229	-29 : 00 : 16.62	(359.9, -0.035)	1.5	26	-56.5	2.31	-3.12
Uncertainties				± 0.1	$^{+54}_{-16}$	± 1.0	± 0.27	± 0.27

Table 2. Stellar photometry, parameters, and abundances

Data	K_S	$H - K_S$	T_{eff} [K]	$\log g$ (dex)	ξ_{mic} [km s^{-1}]	[Fe/H]	[Mg/Fe]	[Si/Fe]	[Ca/Fe]	[Ti/Fe]	[Sc/Fe]
GC10812	10.25	1.63	3817	0.5	2.0	-1.05	0.36	0.39	0.55	0.53	0.44
Uncertainties	± 0.05	± 0.07	± 150	± 0.3	± 0.5	± 0.1	± 0.1	± 0.1	± 0.2	± 0.3	± 0.3

Table 3. Uncertainties due to uncertainties in the stellar parameters

parameter	[Fe/H]	[Mg/Fe]	[Si/Fe]	[Ca/Fe]	[Ti/Fe]	[Sc/Fe]
$\Delta T_{\text{eff}} = \pm 150 \text{ K}$	< 0.02	$^{+0.07}_{-0.02}$	$^{-0.04}_{+0.10}$	$^{+0.16}_{-0.13}$	$^{+0.28}_{-0.22}$	$^{+0.27}_{-0.24}$
$\Delta \log g = \pm 0.3 \text{ dex}$	< 0.02	< 0.02	$^{+0.07}_{-0.03}$	$^{-0.05}_{+0.17}$	$^{-0.03}_{+0.05}$	$^{-0.03}_{+0.05}$
$\Delta \xi_{\text{mic}} = \pm 0.5 \text{ km s}^{-1}$	$^{-0.12}_{+0.10}$	$^{+0.02}_{+0.06}$	$^{-0.01}_{+0.05}$	$^{-0.08}_{+0.13}$	$^{-0.02}_{+0.06}$	$^{-0.06}_{+0.08}$

Table 4. Line list

Element	Wavelength in air [\AA]	Exc. Pot. eV	$\log(gf)$ (cgs)
Mg I	21208.106	6.73	-0.821
Si I	21195.298	7.29	-0.425
Si I	21779.720	6.72	0.418
Si I	21819.711	6.72	0.087
Si I	21874.199	6.72	-0.731
Si I	21879.345	6.72	0.384

Table 4 continued

Table 4 (continued)

Element	Wavelength in air [\AA]	Exc. Pot. eV	$\log(gf)$ (cgs)
Si I	22537.593	6.62	-0.216
Ca I	22626.786	4.68	-0.281
Sc I	21730.452	1.44	-1.880
Sc I	21812.174	1.43	-1.490
Sc I	21842.781	1.43	-1.760
Sc I	22394.695	1.43	-1.180
Ti I	22632.743	1.88	-2.760
Fe I	21124.505	5.33	-1.647

Table 4 continued

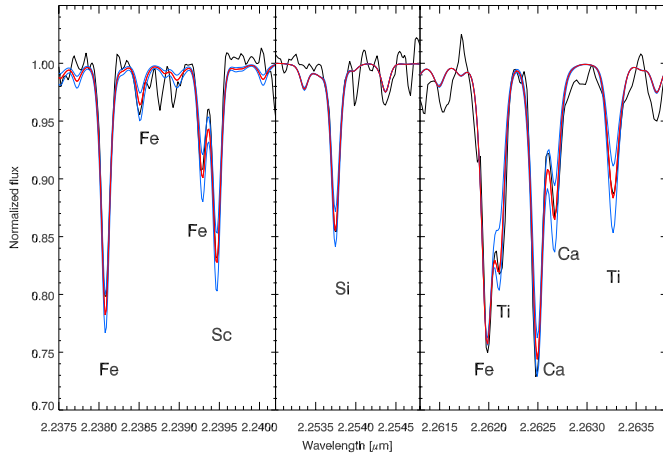


Figure 4. Examples of spectra covering a few of the lines used for the abundance determination. The black curves are the observations, the red one is the best fit model. The blue spectra correspond to ± 0.2 dex in the corresponding abundances, in order to show the sensitivity of these lines to the determined abundances.

Table 4 (*continued*)

Element	Wavelength in air [μ]	Exc. Pot. eV	$\log(gf)$ (cgs)
Fe I	21238.509	4.96	-1.281
Fe I	21779.651	3.64	-4.298
Fe I	21894.983	6.13	-0.135
Fe I	22380.835	5.03	-0.409
Fe I	22392.915	5.10	-1.207
Fe I	22473.263	6.12	0.483
Fe I	22619.873	4.99	-0.362

The abundances of the elements Fe, Mg, Si, Ca, Ti, and Sc are determined from carefully chosen lines. We have restricted our analysis to lines that are on the weak part of the curve of growth, i.e. with equivalent widths of $W < 250 \text{ \AA}$ or $\log W/\lambda < -4.9$. This means that at our resolution of $R = 24,000$, there is an upper limit to the line depth of approximately 0.75 of the continuum. Lines deeper than this will certainly be saturated and will not be as sensitive to the abundance but at the same time more sensitive to the uncertain microturbulence parameters, ξ_{mic} . Our restriction of the analysis to weak lines will ensure a good measurement of the abundances. We also require that the spectral recording around the lines and the form of the continuum is of such high quality that the continuum is traceable.

The final line list is given in Table 4. In the Table the wavelengths, excitation potential, and the line strengths

of the lines used for the abundance determination are given. The entire line list including all lines will be published elsewhere (Thorsbro et al. 2017, in prep.).

Examples of synthetic spectra are shown in Figure 4 and the derived abundances are given in Table 2. The Fe, Si, and Sc abundances are determined from 8, 6, and 4 lines, respectively, whereas the Mg, Ca, and Ti abundances are determined from only one carefully chosen line each. This means that the former abundances are observationally better determined.

The uncertainties in the determination of the abundance ratios, for typical uncertainties in the stellar parameters, are ± 0.1 for $[\text{Fe}/\text{H}]$, $[\text{Mg}/\text{Fe}]$, and $[\text{Si}/\text{Fe}]$, whereas it is ± 0.2 dex for $[\text{Ca}/\text{Fe}]$ and ± 0.3 dex for $[\text{Ti}/\text{Fe}]$ and $[\text{Sc}/\text{Fe}]$, see Table 3. In addition, we estimate random uncertainties of less than 0.05 dex due to the continuum placement. In Figure 4 we show the observed and our best fit spectra, and also synthetic spectra with ± 0.2 dex abundance variations with respect to the best fit solution. The Figure clearly shows that we can derive abundances with overall uncertainties smaller than 0.2 dex.

5. RESULTS

Our derived stellar parameters and their uncertainties for GC10812 are given in Table 2. We find that these parameters place the star in the appropriate location on the Hertzsprung-Russel diagram, as seen in Figure 6. It lies on the red giant branch appropriate for its metallicity, as demonstrated by plotting an old population with the 10 Gyr isochrones of Bressan et al. (2012).

Our derived abundances of Fe, Mg, Si, Ca, Ti and Sc are given in Table 2. We have normalized our derived abundances to the solar abundances of Grevesse et al. (2007): $\log \varepsilon(\text{Mg}) = 7.53$, $\log \varepsilon(\text{Si}) = 7.51$, $\log \varepsilon(\text{Ca}) = 6.31$, $\log \varepsilon(\text{Sc}) = 3.17$, $\log \varepsilon(\text{Ti}) = 5.02$, and $\log \varepsilon(\text{Fe}) = 7.45$.

Typical internal errors in the derived stellar abundances are a few hundredths dex, while the systematic uncertainties due to different assumptions for the stellar parameters are detailed in Table 3 and, on average, amount to 0.1-0.2 dex, often dominated by one of the uncertainties in the stellar parameters.

The derived $[\alpha/\text{Fe}]$ abundance ratios are plotted in Figure 5, together with the corresponding measurements of different samples of giants in the bulge from Gonzalez et al. (2011) and Johnson et al. (2014) by means of optical spectroscopy, as well as measurements in low latitude (innermost 2 degrees) fields from Rich et al. (2007, 2012) and Ryde et al. (2016) by using H and K band IR spectroscopy. In Figure 5 we also reported the measurements of some low mass giants in the Galactic Center region from Ryde & Schultheis (2015) and the average abundance ratios of the three stellar populations of Terzan 5

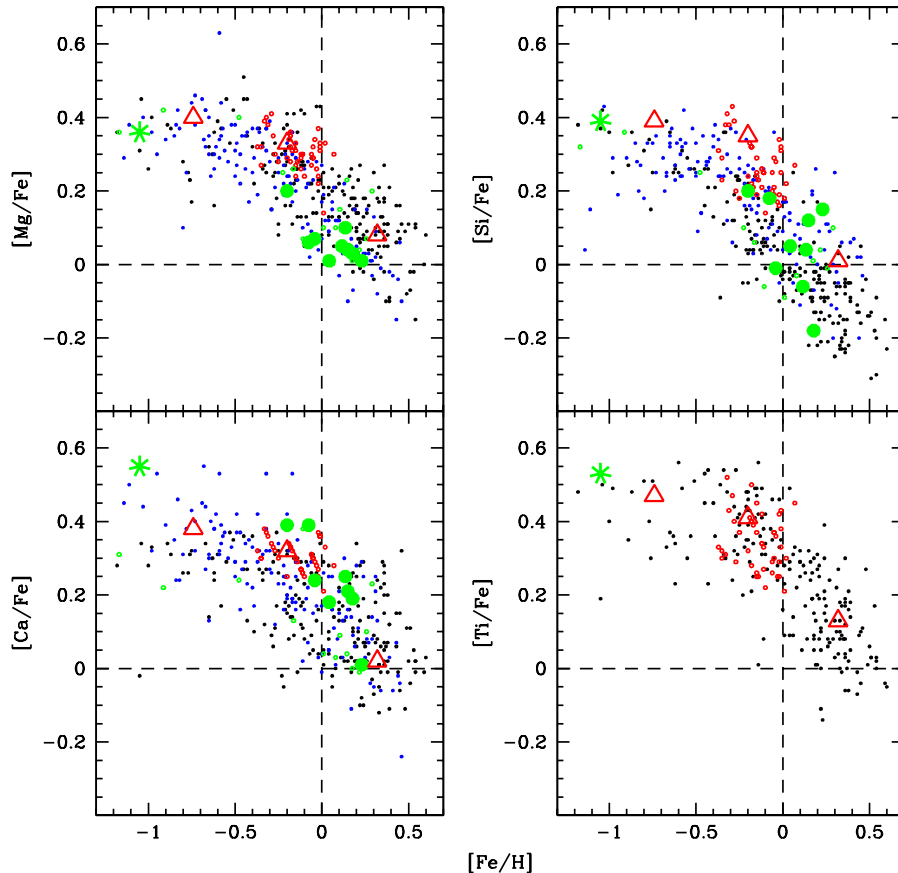


Figure 5. Abundances ratios of $[\text{Mg}/\text{Fe}]$, $[\text{Si}/\text{Fe}]$, $[\text{Ca}/\text{Fe}]$, and $[\text{Ti}/\text{Fe}]$ versus $[\text{Fe}/\text{H}]$ for GC10812 (big green star) and different samples of bulge and Galactic Center giants: [Gonzalez et al. \(2011\)](#) (black dots), [Johnson et al. \(2014\)](#) (blue dots) in the outer bulge from optical spectroscopy; [Rich et al. \(2007, 2012\)](#) (red circles) and [Ryde et al. \(2016\)](#) (green circles) in low latitude bulge fields and [Ryde & Schultheis \(2015\)](#) (big green dots) in the Galactic Center region from IR spectroscopy. The average abundance ratios of the three stellar populations of Terzan 5 from [Origlia et al. \(2011, 2013\)](#) (big red triangles) are also plotted for comparison. We have re-scaled all the abundances to the same solar reference of [Grevesse et al. \(2007\)](#).

at $(l, b) = (3.8^\circ, +1.7^\circ)$ from [Origlia et al. \(2011, 2013\)](#).

We find that the $[\alpha/\text{Fe}]$ abundance ratios of GC10812 are consistent with an enhancement between a factor of two and three with respect to the solar values and fully consistent the values measured in bulge and Galactic Center giants with sub-solar metallicities.

6. DISCUSSION

The best constraint of the 3D location of GC10812 is at 1.5 pc distance from the SgrA* in projected distance on the sky and 26_{-16}^{+54} pc distance in the line-of-sight in front of the Galactic Center. The nuclear cluster has a half-light radius of $178 \pm 51'' \sim 7 \pm 2$ pc ([Fritz et al. 2016](#)) but the nuclear disk extends to about 230 pc ([Launhardt et al. 2002](#)). The dynamics of the star is typical for a Galactic Center star and our orbit calculations show that the star's orbit is constrained within the nuclear disk.

The kinematics strongly favor a galactic center origin

and it is thus rather certain that the star belongs to a nuclear component. The probability of the star being a stray bulge giant is low since most bulge giants are more metal-rich and $[\text{Fe}/\text{H}] \sim -1$ stars are rare in the bulge ([Ness & Freeman 2016](#)). Based on the kinematics and metallicity, the probability of the star being a halo giant is also low since at least in the solar vicinity the halo metallicity in the mean is typically $[\text{Fe}/\text{H}] \sim -1.6$ not -1 ([Ryan & Norris 1991](#)). The relative number density of halo stars in the Galactic Center is difficult to estimate, since there are no measurements of the halo quantitatively even within 8 kpc. Extrapolation can obtain a relevant mass in the center when a broken power-law like, for example, that in [Bland-Hawthorn & Gerhard \(2016\)](#) is used. However, when other parametrizations are used, like an Einasto profile ([Sesar et al. 2013; Xue et al. 2015](#)), the obtained mass is much smaller and irrelevant. Also from a theoretical standpoint a flatter

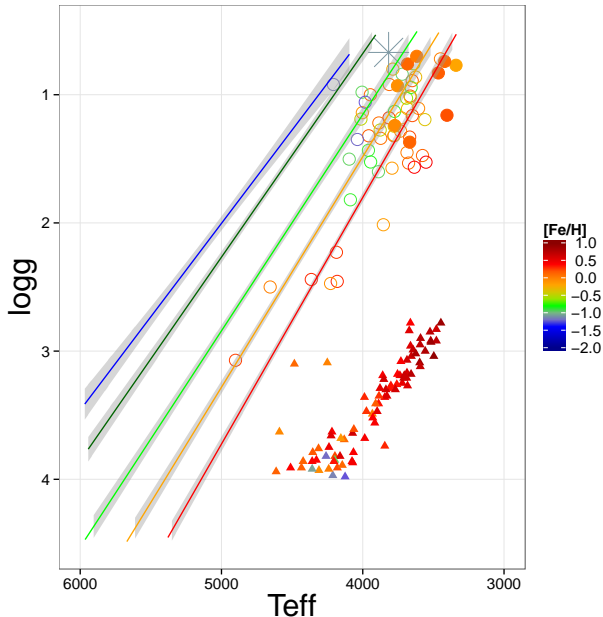


Figure 6. Logarithm of the surface gravities of inner bulge stars plotted versus their effective temperatures and color-coded by their metallicities. The big star is the metal-poor star GC10812 discussed in this paper. The selection of stars in the inner 3° of the bulge from the literature are marked by open circles for the stars from Ryde et al. (2016); Schultheis et al. (2015), by filled circles for the stars within 10 pc projected galactocentric distance from Ryde & Schultheis (2015), and by triangles for the stars discussed in Do et al. (2015). Superimposed are also the 10 Gyr PARSEC isochrones (Bressan et al. 2012) with the corresponding color of the metallicity.

profile is expected, since it is difficult for dwarf galaxies, which probably form the main contributor to the halo, to reach the center of the Milky Way. For example Bullock & Johnston (2005) measure, in their model, a slope of -1 between 3 and 10 kpc, flatter than further out. In summary, we conclude that the probability of GC10812 being a halo star is low.

The metallicity of GC10812 is lower than of most stars in inner bulge. Rich et al. (2007, 2012) find, for example, a dispersion of approximately 0.1 dex around $[\text{Fe}/\text{H}] = -0.05$ to -0.15 . The more recent works of Schultheis et al. (2015); Ryde et al. (2016) found in addition also some metal poor stars with $[\text{Fe}/\text{H}] \approx -1$. They are with $|b| > 0.4^\circ$ all located outside the nuclear disk. Within the nuclear components (disk and cluster) Cunha et al. (2007) find a total spread of 0.16 dex around $[\text{Fe}/\text{H}] = +0.14$ for the luminous giants and supergiants located within 2.2 pc of the Galactic Center. Further, Carr et al. 2000, Ramírez et al. 2000b, and Davies et al. 2009 analyzed high-resolution spectra of supergiant stars in the Galactic Center finding near-solar metallicity. Similarly Ryde & Schultheis (2015) at about 4 arcmin distance from Sgr A* also only detect

a metal-rich component with a total spread of 0.15 dex around $[\text{Fe}/\text{H}] = +0.11$.

The location of the $[\alpha/\text{Fe}]$ abundance ratios versus metallicity for the giant GC10812 is that expected for the metal-poor population in the outer bulge. The $[\text{Mg}/\text{Fe}]$ and $[\text{Si}/\text{Fe}]$ trends of the inner bulge are tight and are indistinguishable from the outer bulge trend, within uncertainties. Although with a larger scatter, this is also true for the $[\text{Ca}/\text{Fe}]$ abundances in the central regions (Cunha et al. 2007; Origlia et al. 2011; Johnson et al. 2014; Ryde et al. 2016). It can, however, be noted that they all follow a higher trend than that determined by Bensby et al. (2013). This might (but not necessarily) arise from greater errors ultimately attributable to the higher uncertainties based on the Ca determination based on the giant star spectra as compared with those based on dwarf spectra (see also the discussion in Gonzalez et al. 2011). Scrutinizing the Ca line used, using more Ca lines, comparing with detailed galactic chemical evolution models, and observing more stars will be needed to investigate and understand the true nature of the $[\text{Ca}/\text{Fe}]$ trend. Our $[\text{Ti}/\text{Fe}]$ determination also has a high uncertainty, mainly arising from the uncertainty in the effective temperature. The value is, however, within errors consistent with the other bulge stars too. Thus, within the uncertainties, the $[\alpha/\text{Fe}]$ we measure for GC10812, cannot be claimed to be different to the rest of the bulge.

The $\log g$ versus T_{eff} location of GC10812 is indicated in Figure 6 with a large asterisk. Superimposed are isochrones color-coded for different metallicities (Bressan et al. 2012). We assume here an age of 10 Gyr. The red line shows the most metal-rich isochrone ($+0.7$ dex). Based on its apparent luminosity, its kinematic membership to one of the nuclear components, its low metallicity, our independent determination of its effective temperature and surface gravity, and its high α -abundance, we are confident that GC10812 is consistent with being a low-mass, old red-giant star in the vicinity of the nuclear cluster.

In the Figure we also plot the locations for a sample of stars in the inner 3° from the Galactic Center from Ryde & Schultheis (2015), Ryde et al. (2016), Schultheis et al. (2015), and Do et al. (2015). The typical uncertainties of temperatures are about ± 150 K while the errors in $\log g$ can be in the order of 0.3-0.5 dex as those were determined photometrically. We note that the isochrones predict too high temperatures, for a given surface gravity, for the most metal-rich stars (> 0.5 dex). One should, however, be aware of the fact that everything at metallicity $> +0.5$ dex needs still to be understood: the metallicities themselves, model atmospheres, and isochrones are all very uncertain and mostly calibrated by extrapolation. Thus, it could be possible that the $\log g$ deter-

mination of the most metal-rich stars are $\sim 0.3-0.5$ dex too high.

Whereas the M giants from Ryde & Schultheis (2015), Ryde et al. (2016) and Schultheis et al. (2015) are situated along the isochrone sequence in Figure 6, the location of the Do et al. (2015) stars is not compatible with the indicated location of the RGB branch from the PARSEC isochrones. These stars are plotted as triangles. As their extinction is typically that of stars in the Galactic Center, we believe that their surface gravities are about two to three order of magnitudes too high. Also, the metal-poor stars discussed in Do et al. (2015), are orders of magnitude away from the expected isochrones.

The work of Do et al. (2015) obtained integral-field, moderate-resolution spectroscopy for scores of stars in the central cluster behind AO. They did not claim to undertake a full high-resolution abundance analysis and were aware of potentially significant uncertainties in their methods. Their stated uncertainty in $\log g$ is 0.91 dex. The main effect of decreasing the surface gravity in a synthetic spectrum calculation is the decreased continuous opacity, which generally increases line strengths. In the simultaneous fit of the stellar parameters by Do et al. (2015), the temperature and metallicity determinations might therefore also be affected by this large uncertainty. We agree with the assessment of Do et al. (2015) that additional observations at high spectral resolution would be required to confirm the low metallicities ($[\text{Fe}/\text{H}] \sim -1$) claimed for the five stars in the nuclear cluster. Likewise, the high-metallicity stars found by Do et al. (2015), which have nominal metallicities up to $[\text{Fe}/\text{H}] = +1.0$ dex, need to be confirmed.

The similarity between GC10812 and the rest of the inner bulge, would suggest a homogeneous star-formation history in the entire bulge. There is a clear connection with the bulge and the Center. Thus, our results argues for the Center being in the context of the bulge over most of its history rather than very distinct.

7. CONCLUSIONS

In targeting the Milky Way nuclear star cluster we have observed the most metal-poor giant (GC10812) yet in the vicinity of the Galactic Center. A careful analysis of its 3-dimensional location, locates it at 26_{-16}^{+54} pc in front of the Galactic Center and at a projected distance of 1.5 pc to the North-West. This line of sight position and orbit integration makes it unlikely that the star belongs the most central component, the nuclear cluster. However, the orbit integration also shows that the star very likely does not leave the nuclear disk. Thus, the star very likely belongs to a nuclear component.

The metallicity and abundances are determined from a detailed abundance analysis based on $R = 24000$ Keck/NIRSPEC spectra. The $[\text{Fe}/\text{H}] = -1.05 \pm 0.10$ is

the lowest measured and confirmed metallicity of a star from the nuclear components. It is unexpected and differs from earlier measurements. We can, however, still conclude that there is no evidence hitherto that there are metal-poor stars (e.g. originating in globular cluster in-spiraling to the Galactic Center (Tremaine et al. 1975; Capuzzo-Dolcetta & Miocchi 2008)) in the nuclear star cluster. The $[\alpha/\text{Fe}]$ -element enhancement of $\sim +0.4$ follows the trend of the outer bulge.

GC10812 is by virtue of its 3D kinematics a likely member of the central disk/cluster system. It also exhibits the metal poor, alpha enhanced hallmarks of an old, metal poor giant. The existence of an old population in the Galactic Center has been well established from the robust presence of a red clump population (Figer et al. 2004) as well as the analysis of star formation history by Pfuhl et al. (2011). It will be important going forward to explore the full abundance distribution of this old population, as well as that of the $\sim 10^8$ yr population responsible for the supergiants. Such studies will lay the foundation for applying models of chemical evolution to this very interesting region of the Milky Way.

We have demonstrated that K band spectroscopy of individual giants at high spectral resolution offers a path forward enabling exploration of the chemistry of the central cluster. This has the potential to elucidate the system's star formation and enrichment history as well as its relationship with the central 100 pc of the bulge/bar system.

We would like to thank the referee for an insightful and careful report which improved the paper. Nikolai Piskunov is thanked for developing the spectral synthesis code, SME, to handle fully spherical-symmetric problems. Asli Pehlivan is thanked for providing atomic data on Mg lines prior to its publication. N.R. acknowledges support from the Swedish Research Council, VR (project number 621-2014-5640), and Funds from Kungl. Fysiografiska Sllskapet i Lund (Stiftelsen Walter Gyllenbergs fond and Mrta och Erik Holmbergs donation). R.M.R. acknowledges support from grant AST-1413755 from the US National Science Foundation. L.O. acknowledges PRIN INAF 2014 - CRA 1.05.01.94.11: "Probing the internal dynamics of globular clusters. The first, comprehensive radial mapping of individual star kinematics with the new generation of multi-object spectrographs (PI: L. Origlia). S.C. acknowledges support from the Research Center for Astronomy, Academy of Athens. The authors wish to recognize and acknowledge the very significant cultural role and reverence that the summit of Mauna Kea has always had within the indigenous Hawaiian community. We are most fortunate

to have the opportunity to conduct observations from this mountain.

REFERENCES

- Ahn, C. P., Alexandroff, R., Allende Prieto, C., et al. 2014, *ApJS*, **211**, 17
- Anstee, S. D., & O’Mara, B. J. 1991, *MNRAS*, **253**, 549
- Baade, W. 1951, Publications of Michigan Observatory, 10, 7
- Barklem, P. S., & O’Mara, B. J. 1998, *MNRAS*, **300**, 863
- Bensby, T., Yee, J. C., Feltzing, S., et al. 2013, *A&A*, **549**, A147
- Bland-Hawthorn, J., & Gerhard, O. 2016, ArXiv e-prints, [arXiv:1602.07702](https://arxiv.org/abs/1602.07702)
- Blum, R. D., Ramírez, S. V., Sellgren, K., & Olsen, K. 2003, *ApJ*, **597**, 323
- Bonnet, H., Ströbele, S., Biancat-Marchet, F., et al. 2003, in *Proc. SPIE, Vol. 4839, Adaptive Optical System Technologies II*, ed. P. L. Wizinowich & D. Bonaccini, 329
- Bressan, A., Marigo, P., Girardi, L., et al. 2012, *MNRAS*, **427**, 127
- Bullock, J. S., & Johnston, K. V. 2005, *ApJ*, **635**, 931
- Capuzzo-Dolcetta, R., & Miocchi, P. 2008, *ApJ*, **681**, 1136
- Cardelli, J. A., Clayton, G. C., & Mathis, J. S. 1989, *ApJ*, **345**, 245
- Carr, J. S., Sellgren, K., & Balachandran, S. C. 2000, *ApJ*, **530**, 307
- Chatzopoulos, S., Fritz, T. K., Gerhard, O., et al. 2015a, *MNRAS*, **447**, 948
- Chatzopoulos, S., Gerhard, O., Fritz, T. K., et al. 2015b, *MNRAS*, **453**, 939
- Cunha, K., Sellgren, K., Smith, V. V., et al. 2007, *ApJ*, **669**, 1011
- Davies, B., Origlia, L., Kudritzki, R.-P., et al. 2009, *ApJ*, **694**, 46
- Do, T., Kerzendorf, W., Winsor, N., et al. 2015, ArXiv e-prints, [arXiv:1506.07891](https://arxiv.org/abs/1506.07891)
- Eisenhauer, F., Abuter, R., Bickert, K., et al. 2003, in *Proc. SPIE, Vol. 4841, Instrument Design and Performance for Optical/Infrared Ground-based Telescopes*, ed. M. Iye & A. F. M. Moorwood, 1548
- Figer, D. F., Rich, R. M., Kim, S. S., Morris, M., & Serabyn, E. 2004, *ApJ*, **601**, 319
- Fritz, T. K., Gillessen, S., Dodds-Eden, K., et al. 2011, *ApJ*, **737**, 73
- Fritz, T. K., Chatzopoulos, S., Gerhard, O., et al. 2016, *ApJ*, **821**, 44
- Fulbright, J. P., McWilliam, A., & Rich, R. M. 2006, *ApJ*, **636**, 821
- Gonzalez, O. A., Rejkuba, M., Zoccali, M., et al. 2011, *A&A*, **530**, A54
- Gonzalez, O. A., Zoccali, M., Vasquez, S., et al. 2015, *A&A*, **584**, A46
- Goorvitch, D. 1994, *ApJSS*, **95**, 535
- Grevesse, N., Asplund, M., & Sauval, A. J. 2007, *SSRv*, **130**, 105
- Gustafsson, B., Edvardsson, B., Eriksson, K., et al. 2008, *A&A*, **486**, 951
- Hinkle, K., Wallace, L., & Livingston, W. C. 1995, Infrared atlas of the Arcturus spectrum, 0.9-5.3 microns (San Francisco, Calif. : Astronomical Society of the Pacific, 1995.)
- Houdashelt, M. L., Bell, R. A., & Sweigart, A. V. 2000, *AJ*, **119**, 1448
- Howes, L. M., Casey, A. R., Asplund, M., et al. 2015, *Nature*, **527**, 484
- Jørgensen, U. G., & Larsson, M. 1990, *A&A*, **238**, 424
- Johnson, C. I., Rich, R. M., Fulbright, J. P., Valenti, E., & McWilliam, A. 2011, *ApJ*, **732**, 108
- Johnson, C. I., Rich, R. M., Kobayashi, C., Kunder, A., & Koch, A. 2014, *THE ASTRONOMICAL JOURNAL*, **148**, 67
- Johnson, C. I., Rich, R. M., Kobayashi, C., et al. 2013, *ApJ*, **765**, 157
- Kim, S., Prato, L., & McLean, I. 2015, REDSPEC: NIRSPEC data reduction, Astrophysics Source Code Library, [ascl:1507.017](https://ui.adsabs.org/abs/2015ascl.1507.017)
- Koch, A., McWilliam, A., Preston, G. W., & Thompson, I. B. 2016, *A&A*, **587**, A124
- Kupka, F., Piskunov, N., Ryabchikova, T. A., Stempels, H. C., & Weiss, W. W. 1999, *A&AS*, **138**, 119
- Kupka, F. G., Ryabchikova, T. A., Piskunov, N. E., Stempels, H. C., & Weiss, W. W. 2000, *Baltic Astronomy*, **9**, 590
- Launhardt, R., Zylka, R., & Mezger, P. G. 2002, *A&A*, **384**, 112
- Lawrence, A., Warren, S. J., Almaini, O., et al. 2013, *VizieR Online Data Catalog*, 2319, 0
- Livingston, W., & Wallace, L. 1991, An atlas of the solar spectrum in the infrared from 1850 to 9000 cm⁻¹ (1.1 to 5.4 micrometer) (NSO Technical Report, Tucson: National Solar Observatory, National Optical Astronomy Observatory, 1991)
- Matsunaga, N., Kawadu, T., Nishiyama, S., et al. 2009, *MNRAS*, **399**, 1709
- McLean, I. S. 2005, in *High Resolution Infrared Spectroscopy in Astronomy*, ed. H. U. Käuff, R. Siebenmorgen, & A. F. M. Moorwood, 25
- Nassau, J. J., & Blanco, V. M. 1958, *ApJ*, **128**, 46
- Ness, M., & Freeman, K. 2016, *PASA*, **33**, e022
- Ness, M., Freeman, K., Athanassoula, E., et al. 2013, *MNRAS*, **430**, 836
- Nishiyama, S., Tamura, M., Hatano, H., et al. 2009, *ApJ*, **696**, 1407
- Omont, A., Ganesh, S., Alard, C., et al. 1999, *A&A*, **348**, 755
- Origlia, L., Massari, D., Rich, R. M., et al. 2013, *ApJL*, **779**, L5
- Origlia, L., Rich, R. M., Ferraro, F. R., et al. 2011, *ApJL*, **726**, L20
- Pehlivan, A., Nilsson, H., & Hartman, H. 2015, *A&A*, **582**, A98
- Pfuhl, O., Fritz, T. K., Zilka, M., et al. 2011, *ApJ*, **741**, 108
- Piskunov, N., & Valenti, J. A. 2016, ArXiv e-prints, [arXiv:1606.06073](https://arxiv.org/abs/1606.06073) [[astro-ph.IM](https://arxiv.org/abs/1606.06073)]
- Piskunov, N. E., Kupka, F., Ryabchikova, T. A., Weiss, W. W., & Jeffery, C. S. 1995, *A&AS*, **112**, 525
- Ramírez, I., & Allende Prieto, C. 2011, *ApJ*, **743**, 135
- Ramirez, S. V., Depoy, D. L., Frogel, J. A., Sellgren, K., & Blum, R. D. 1997, *AJ*, **113**, 1411
- Ramírez, S. V., Sellgren, K., Carr, J. S., et al. 2000a, *ApJ*, **537**, 205
- Ramírez, S. V., Stephens, A. W., Frogel, J. A., & DePoy, D. L. 2000b, *AJ*, **120**, 833
- Rich, R. M. 1988, *AJ*, **95**, 828
- Rich, R. M., Origlia, L., & Valenti, E. 2007, *ApJL*, **665**, L119
- . 2012, *ApJ*, **746**, 59
- Ryabchikova, T., Piskunov, N., Kurucz, R. L., et al. 2015, *PhyS*, **90**, 054005
- Ryabchikova, T. A., Piskunov, N. E., Kupka, F., & Weiss, W. W. 1997, *Baltic Astronomy*, **6**, 244
- Ryan, S. G., & Norris, J. E. 1991, *AJ*, **101**, 1865
- Ryde, N., & Schultheis, M. 2015, *A&A*, **573**, A14
- Ryde, N., Schultheis, M., Grieco, V., et al. 2016, *AJ*, **151**, 1
- Schödel, R., Feldmeier, A., Kunneriath, D., et al. 2014, *A&A*, **566**, A47
- Schödel, R., Najarro, F., Muzic, K., & Eckart, A. 2010, *A&A*, **511**, A18
- Schultheis, M., Ryde, N., & Nandakumar, G. 2016, ArXiv e-prints, [arXiv:1603.02633](https://arxiv.org/abs/1603.02633) [[astro-ph.SR](https://arxiv.org/abs/1603.02633)]

- Schultheis, M., Chen, B. Q., Jiang, B. W., et al. 2014, [A&A](#), **566**, [A120](#)
- Schultheis, M., Cunha, K., Zasowski, G., et al. 2015, [A&A](#), **584**, [A45](#)
- Sesar, B., Ivezić, Ž., Stuart, J. S., et al. 2013, [AJ](#), **146**, **21**
- Tiede, G. P., Frogel, J. A., & Terndrup, D. M. 1995, [AJ](#), **110**, **2788**
- Tody, D. 1993, in ASP Conf. Ser. 52: Astronomical Data Analysis Software and Systems II, ed. R. J. Hanisch, R. J. V. Brissenden, & J. Barnes, 173
- Tremaine, S. D., Ostriker, J. P., & Spitzer, Jr., L. 1975, [ApJ](#), **196**, **407**
- Tsuji, T. 2008, [A&A](#), **489**, **1271**
- Valenti, J. A., & Piskunov, N. 1996, [A&AS](#), **118**, 595
- . 2012, SME: Spectroscopy Made Easy, [ascl:1202.013](#), astrophysics Source Code Library
- Xue, X.-X., Rix, H.-W., Ma, Z., et al. 2015, [ApJ](#), **809**, **144**
- Zoccali, M., Hill, V., Lecureur, A., et al. 2008, [A&A](#), **486**, **177**